A minimal hepatocyte growth factor mimic acting as a powerful agonist of the MET receptor tyrosine kinase for regeneration of epithelial tissues and organs.

Short Title: Kringle 1 dimer as a minimal MET agonist.

Authors

Bérénice Leclercq[1*], Giovanni de Nola[2*], Alexandra Mougel[1], Solenne Dezitter-Tarron[3], Claire Simonneau[4], Federico Forneris[5], Eric Adriaenssens[1], Hervé Drobecq[1], Ermanno Gherardi[6], Oleg Melnyk[1], Hugo de Jonge[6#], and Jérôme Vicogne[1#].

1. Univ. Lille, CNRS, Inserm, CHU Lille, Institut Pasteur de Lille, U1019 - UMR 9017 - CIIL - Center for Infection and Immunity of Lille, F-59000 Lille, France.

2. Department of Neurobiology, Harvard Medical School, Boston, MA 02115, USA

3. University of Lille, U1286 Inserm, Institute for Translational Research in Inflammation Infinite, CHU Lille, F-59000 Lille, France.

4. Roche Innovation Center Basel, Zürich, Switzerland

5. The Armenise-Harvard Laboratory of Structural Biology, Dept. Biology and Biotechnology - University of Pavia, via Ferrata 9, 27100 Pavia, Italy

6. Department of Molecular Medicine, Pavia University Immunology and General Pathology section, via Ferrata 9, 27100 Pavia (PV), Italy

* Joint authorship

co-corresponding: e-mail: jerome.vicogne@ibl.cnrs.fr; hugo.dejonge@unipv.it

Abbreviations

ALPHA: amplified luminescent proximity homogenous assay

COPD: chronic obstructive pulmonary disease

PBS: phosphate buffer saline

rcf: relative centrifugal force,

Abstract

Degenerative diseases of major internal epithelial organs such as liver, lung and kidney account for more than one third of mortality worldwide. The huge demand for drugs able to limit epithelial tissue degradation and eventually restore its functionality, place mimics of the hepatocyte growth factor/scatter factor (HGF/SF), the physiological ligand for the MET receptor tyrosine kinase, at the forefront of potential drug candidates. HGF/SF is a growth and motility factor with essential physiological roles in development and regeneration of epithelial organs. Unfortunately, HGF/SF itself is unsuitable for therapy because naturally the factor acts only locally as a morphogen and chemoattractant and has poor in vivo distribution and shelf life profile. We have therefore designed, produced, solved the crystal structure and characterized the biochemical and biological properties of K1K1, a new engineered fragment of HGF/SF for applications in tissue/organ regeneration. K1K1, a covalent dimer of the first kringle domain of HGF/SF, is recombinantly produced in bacterial cells, shows superior stability at physiological pH and ionic strength and is a potent receptor agonist as demonstrated in a wide range of biological assays with cells in culture and initial in vivo studies. K1K1 has broad potential in regenerative medicine with diseases such as acute liver failure, non-alcoholic steatohepatitis, chronic obstructive pulmonary disease and acute kidney injury.

Key words

HGF/SF, MET receptor agonist, recombinant protein engineering, regeneration.

Introduction

The degree of control that mankind has achieved over a number of infectious diseases, combined with increased food supply, has more than doubled life expectancy in less than two hundred years and caused a dramatic shift in mortality towards cancer and degenerative diseases[1]. The consequences of this major epidemiological transition are far reaching and, in the words of the latest WHO report on Noncommunicable Diseases*: the human, social and economic costs of degenerative diseases of the central nervous system and major internal organs will continue to grow and overwhelm the capacity of countries to address them unless more effective preventable measures and treatments will be developed*[2]. The development of effective therapies for tissue/organ regeneration thus clearly constitute both an urgent need and a major challenge, which can be met through greater

understanding and control of the cellular dynamics of tissue regeneration and the molecules that control such processes.

Cell-based therapies for several degenerative diseases can be safe and effective but cannot extend to diseases affecting millions of individuals. Alternative approaches are needed for common, degenerative diseases of major, internal epithelial organs such as alcoholic and non-alcoholic fat liver disease (AFLD and NAFLD) leading to chronic liver failure, chronic obstructive pulmonary disease (COPD) and acute kidney injury (AKI) leading to chronic renal failure. These diseases affect millions of patients worldwide, are major causes of mortality[3] and impact dramatically on the financial resources of the health systems of rich as well as developing countries.

Regardless of initial cause of cell/tissue damage: virus, alcohol or dietary fat in the case of liver disease, tobacco and/or air pollution for COPD, chemicals or drugs for AKI, the response to damage of different epithelial organs display remarkable similarities: when regeneration fails to compensate for the loss of parenchymal cells, this imbalance triggers a chronic inflammatory tissue response and the proliferation/activation of non-epithelial cell populations - fibroblasts and myofibroblasts - responsible for the synthesis of extracellular matrix and fibrosis leading to loss of organ function[4]. The key to the control of chronic diseases of epithelial organs therefore, short of removing initial causes of damage (alcohol, tobacco, chemicals) or targeting therapeutically other causes of damage (viruses) is to promote regeneration of parenchymal cells in early disease stages prior to the onset of chronic inflammation and fibrosis. Complementary, the prospect of enhancing therapeutically the regenerative capabilities of epithelial organs thus preventing the onset of chronic inflammation and fibrosis by harnessing the full regenerative potential of endogenous, tissue progenitor or differentiated cells is promising and may reach large patient populations.

We propose to implement this paradigm by reshaping - by protein engineering - the polypeptide growth/motility factor and potent epithelial morphogen hepatocyte growth factor/scatter factor (HGF/SF)[5,6] for regenerative medicine. HGF/SF is produced by fibroblasts and other mesenchymal cells that acts in a paracrine manner on target epithelial cells through binding to MET, a receptor tyrosine kinase[7,8]. The evidence for a physiological role of HGF/SF-MET signalling in development and regeneration of liver, lung and kidney is extensive and compelling. HGF/SF-MET is required for lung[9] and kidney[10] development, for survival and regeneration of kidney tubular cells after injury[11] and above all HGF/SF inhibits both lung[12,13] and kidney[14] fibrosis after injury. These data establish HGF/SF as a key effector of epithelial morphogenesis and a protein with unique therapeutic potential for regeneration of epithelial tissues and organs.

There are several drawbacks, however, in using HGF/SF, the natural MET ligand, for therapy. HGF/SF has a very short half-life[15] and is unstable in physiological buffers[16]. Moreover, it has a high affinity for heparan sulphate proteoglycans (HSPG)[17], thereby limiting its tissue/organ penetration and distribution. These properties reflect the nature of HGF/SF as a potent, locally acting chemoattractant, growth factor and morphogen, but constitute appreciable limitations in a therapeutic setting. Here we

overcome these limitations by reshaping HGF/SF for therapy through design and synthesis of a novel, ligand-based, minimal MET agonist.

HGF/SF is structurally related to the blood proteinase plasminogen. Its signalling-active two-chain conformation consists of a larger α-chain containing five protein domains, an N-terminal (N) domain homologous to plasminogen activation peptide and four kringle (K) domains, and a smaller β-chain containing the C-terminal domain homologous to the catalytic domain of serine proteinases (SPH). The evolutionary conserved proteolytic mechanism of activation of the complex blood proteinases and HGF/SF provides a powerful link between the coagulation/fibrinolytic pathways and organ regeneration. Pro-HGF/SF is activated by several of enzymes of the coagulation cascade, as well as by two membrane serine proteinases (matriptase and hepsin)[18]. Thus, in embryogenesis, in tissue remodelling and at sites of tissue damage, activation of the clotting/fibrinolytic pathways causes activation of pro-HGF/SF promoting survival and regeneration of parenchymal cells.

MET is also synthesised as a single chain precursor and is cleaved by furin in the endoplasmic reticulum yielding an N-terminal α-chain and a larger β-chain. The large ectodomain of the MET tyrosine kinase consists of two main parts: a large N-terminal SEMA domain responsible for ligand binding on the top of a stalk structure that includes a small cystine-rich (CR) domain and four copies of immunoglobulin-like (IG) domains[19]. Activation of MET results in the recruitment of scaffolding proteins such as Gab1 and Grb2, which activate Shp2, Ras and ERK/MAPK causing: (i) activation of cell survival pathways through inhibition of caspase-9 and Bad, (ii) changes in gene expression of cell-cycle regulators (such as pRB, Cdk6 and p27), (iii) expression and post-translational activation of matrix metalloproteinases (MMPs) and urokinase (u-PA) leading to alterations of the cytoskeleton necessary for cell migration and division, and (v) changes in expression of cadherins, Arp2/3, N-WASP, paxillin, integrins and focal adhesion kinase (FAK) essential for cell migration. Globally, HGF/SF-MET signalling causes cell survival, division, migration and a complex morphogenetic programme underlying tissue regeneration[20,21].

In earlier studies, we defined the structures of an N-terminal fragment of HGF/SF (NK1) that shows good agonist activities and harbours the high-affinity binding site for MET (27). Building upon our earlier crystallographic and protein engineering studies[19,22–28] and recent insights on the role of kringle 1 domain (K1) in agonistic activity[29], we hypothesized that two K1 domains in tandem forming the covalent K1K1 dimer could behave as a minimal receptor agonist endowed with appropriate properties for acting in vivo. Here we report the design of K1K1 protein, its expression in bacterial cells and its extensive structural, biochemical and biological characterization. These studies pave the way for more extensive testing of K1K1 in vivo specific models for application in acute and chronic degenerative diseases of liver, lung and kidney as well as application in neurodegenerative disorders such as ALS and MS[30–32].

Material and Methods

Cloning of K1K1 and K1K1 variants

The cDNA encoding K1K1 and K1K1H6 was generated using a fusion PCR reaction after separate PCR amplification of two K1 domains from a wild-type human NK1 template. The forward primer, ATCATCCCATGGCCATTAGAAACTGCATCATTGGTAAAGGACG, was used to amplify the first kringle domain introducing a 5' NcoI restriction site. The reverse primer for the first K1, TTCAACTTCTGAACACTGAGGA, was used to introduce the linker sequence S E V E placed in-between the two K1 domains. S E V E is naturally found in HGF/SF in between K1 and K2 domains. The forward primer for the second K1 domain, TCAGAAGTTGAATGCATCATTGGTAAAGGACG, introduces the fusion-overlap with the SEVE linker sequence. A reverse primer with or without a six-histidine tag, ACAGCGGCCGCTCATCAATGATGATGATGATGATGTTCAACTTCTGAACACTGAGGA and ACAGCGGCCGCTCATCATTCAACTTCACTACACTGAGGAAT respectively, introduced two stop codons followed by a NotI restriction site. Following the fusion PCR reaction, the product was digested with NcoI and NotI and ligated into the pET45b(+) expression plasmid (Novagen/EMD Millipore). Integration in the pET45b(+) MCS introduced the additional amino acid sequence M A I R N upstream of the first cysteine of K1 domain, as naturally found in HGF/SF.

The heparin mutants S2 and S4 were based on existing kringle-variant NK1 templates. These templates introduced the reverse-charge amino acid substitutions K10E, R12E, K93E, R95E for K1K1S2 and K10E, R12E, K48E, R59E, K93E, R95E, K131E, R142E for K1K1S4.

Protein expression

Recombinant human NK1 protein (residues 28-209) was expressed in *Pichia pastoris* and purified as described in Chirgadze et al., 1999[23]. Recombinant human MET567 was expressed in CHO Lec 3.2.8.1 cells and purified as described in Gherardi et al., 2003[19]. Human HGF/SF was stably expressed in NS0 myeloma cells and purified as described in Gherardi et al., 2006[33].

For the expression of K1K1 and K1K1 variants, a single colony of freshly transformed *E. coli* BL21(DE3) was used to inoculate an overnight 5 mL Luria broth (LB) culture containing 100 μg/mL of ampicillin. This culture was used to inoculate 500 mL of LB with ampicillin shaking at 250 rpm and grown to an optical density (600 nm) of 0.6-0.8 at 37 °C. The culture was then cooled down to 18 °C while shaking after which IPTG was added to a final concentration of 0.1 mM. The culture was grown at 18 °C with shaking for 24 h after which the bacterial cells were harvested by centrifugation for 30 min at 10,000 rcf at 4 °C and the cell pellet was stored at -80 °C.

K1K1 extraction from inclusion bodies

The frozen bacterial cell pellet was thawed on ice and resuspended in 25 mL 50 mM Tris pH 8.5, 500 mM NaCl, with the addition of one tablet of cOmplete™ EDTA-free Protease Inhibitor Cocktail (Roche), 1 unit of Pierce Universal Nuclease and 10 μg of lysozyme. The suspension was incubated rotating at

4 °C for 30 min before being placed on ice and sonicated using ten pulses of 30 s with 60 s pause in between using a Sonic Ruptor 400 (Omni International) with a OR-T-750 tip at 100% power output. The suspension was centrifuged at 10,000 rcf for 10 min, the supernatant discarded, and the pellet resuspended in 25 mL 50 mM Tris pH 8.5, 500 mM NaCl with 0.4% Triton X-100 using a glass Potter-Elvehjem tube and PTFE pestle. The suspension was incubated at 4 °C rotating for 30 min after which it was centrifuged at 10,000 rcf for 10 min, the supernatant discarded, and the pellet resuspended in 25 mL 50 mM Tris pH 8.5, 500 mM NaCl with 0.025% NP40 using the Potter-Elvehjem tube and pestle. The suspension was again incubated at 4 °C rotating for 30 min, centrifuged for 10 min at 10,000 rcf, the supernatant discarded, and the pellet resuspended in 25 mL 50 mM Tris pH 8.5, 500 mM NaCl using the Potter-Elvehjem tube and pestle. The suspension was once more incubated at 4 °C rotating for 30 min, centrifuged at 10,000 rcf for 10 min, and the supernatant discarded. The final pellet was resuspended in 20 mL 50 mM Tris pH 8.5, 500 mM NaCl, 2 M arginine, 0.5 mM GSSG, 5 mM GSH. This suspension was incubated for three days at 4 °C on a rotary wheel.

K1K1 purification

After three days of incubation in Tris buffer with arginine, the inclusion body suspension was centrifuged at 20,000 rcf for 30 min at 4 °C. The supernatant was transferred to a new centrifuge tube and centrifuged again at 20,000 rcf for an additional 30 min at 4 °C. Unless a pellet was visible, in which case a third centrifugation was performed in a new tube, the cleared supernatant was diluted 100 times in 2 L of 50 mM Tris pH 7.4, 150 mM NaCl and filtered. The diluted supernatant was loaded onto a 5 mL Heparin HiTrap™ column (GE Healthcare) and eluted with a gradient up to 1 M NaCl, in 50 mM Tris pH 7.4. Peak fractions were pooled, concentrated and loaded on a HiLoad® 16/600 Superdex 200 pg column (GE Healthcare) equilibrated in 50 mM Tris pH 7.4, 500 mM NaCl. Peak fractions were pooled and concentrated to 5 mg/mL before being used or stored after flash freezing. For K1K1S2 and K1K1S4, instead of Heparin HiTrap™ column, the first step purification was done on a 5 mL HisTrap™ HP column (GE Healthcare).

Protein crystallization and x-ray diffraction

For protein crystallization, K1K1 and K1K1H6 were dialyzed in 10 mM Tris pH 8.5, 100 mM NaCl and concentrated to 12 mg/mL and 11.8 mg/mL respectively. A pre-crystallization screen (PCT, Hampton Research) was performed to confirm these concentrations were favorable for crystallization after which 48-well sitting-drop plates (Hampton Research) were set up using Crystal screen 1 (Hampton Research), JCSG-plus™ (Molecular Dimension) and Morpheus® (Molecular Dimensions) crystallization screens. After overnight incubation at 17 °C, the first crystals appeared in the Morpheus® screen in condition C11 consisting of 100 mM Tris/Bicine pH 8.5, 90 mM sodium nitrate, 90 mM sodium phosphate dibasic, 90 mM ammonium sulphate, 20% v/v glycerol, 10% w/v PEG4000. Further

optimization was performed with different protein to crystallization solution ratios (1:2, 1:1, 2:1) in a 24-well plate using hanging drop. After 24 h, good crystals were obtained in a 2:1 protein-to-solution ratio condition. In addition to the cryo-protection intrinsic to the Morpheus® screen, additional glycerol was added up to 25% of the final volume before crystals were collected using a CryoLoop (Hampton Research) and flash frozen and stored in liquid nitrogen. Data was collected at the ESRF in Grenoble, France, at beamline at ID23-1 and was solved by molecular replacement using the NK1 kringle domain as a search model resulting in a structure with a resolution of 1.6A and an R/Rfree of 20.8/24.3% for K1K1 and a structure with a resolution of 1.8A and an R/Rfree of 18/22% for K1K1H6. Both proteins crystalized in space group P21.

SAXS

Solution scattering data were collected at ESRF BM29 using a sec-1 frame rate on Pilatus 1 M detector located at a fixed distance of 2.87 m from the sample, allowing a global q range of 0.03-4.5 nm with a wavelength of 0.01 nm. SEC-SAXS experiments were carried out using Nexera High Pressure Liquid/Chromatography (HPLC; Shimadzu) system connected online to SAXS sample capillary. For these experiments, 35 μL of each sample at the concentrations indicated in the Table were injected into a Superdex 200 PC 3.2/300 Increase column (GE Healthcare), pre-equilibrated with 25 mM Tris pH 7.4, 150 mM NaCl. Frames corresponding to protein peaks were identified, blank subtracted and averaged using CHROMIXS2. Radii of gyration (Rg), molar mass estimates and distance distribution functions P(r) were computed using the ATSAS package3 in PRIMUS. Modelling of flexible loops and glycosylation were carried out using COOT, CORAL and SASREF. Comparison of experimental SAXS data and 3D models from structural models was performed using CRYSOL. A summary of SAXS data collection and analysis results is shown in Table 1.

Table 1. Summary of SAXS data analysis.

	K1K1	MET567	K1K1+MET567
Data Collection			
BeamLine	ESRF BM29	ESRF BM29	ESRF BM29
Beam energy (keV)	12.5	12.5	12.5
Sample-detector distance (m)	2.867	2.867	2.867
Exposure time (s)	1	1	1
Sample cell thickness (mm)	1	1	1
Sample concentration (mg/mL)	8.5 mg/mL	7.6 mg/mL	12.4 mg/mL
Temperature (°C)	20	20	20
Final q range (nm^{-1})	0.01 - 4	0.01 - 4	0.01 - 4
Data Analysis			
Points used for Guinier analysis	1-94	11-48	2-28
Guinier qR_g limits	1.30	0.97	0.99
Guinier R_g (nm)	2.22	3.23	3.78
I(0) (mm^{-1})	14.8 ± 0.01	64.9 ± 0.04	69.9 ± 0.08
D_{max} (nm)	6.6	11.5	14.2
MW estimation (V_c based) (kDa)	16.5	66.2	83.4

AlphaScreen™ MET binding assay.

Saturation assays for binding of K1K1H6 to recombinant MET-Fc protein were performed in 384-well microtiter plates (OptiPlate™-384, PerkinElmer©, CA, USA, 50 µL of final reaction volume). Final concentrations were 0-300 nM for K1K1H6, 0-10 nM for hMET-Fc (8614-MT-100, R&D Systems), 10 µg/mL for Ni-NTA coated donor beads and protein A-conjugated acceptor beads. The buffer used for preparing all protein solutions and the bead suspensions was PBS (10 mM phosphate buffer pH 7.4, 148 mM NaCl, 2mM KCl), 5 mM HEPES pH 7.4, 0.1% BSA. K1K1H6 (10 µL, 0-1.5 µM) was mixed with solutions of MET-Fc (10 µL, 0-50 nM). The mixture was incubated for 10 min (final volume 15 µL). Protein A-conjugated acceptor beads (10 µL, 50 µg/mL) were then added to the vials. The plate was incubated at 23°C for 30 min in a dark box. Finally, Ni-NTA coated donor beads (10 µL, 50 µg/mL) were added and the plate was further incubated at 23°C for 60 min in a dark box. The emitted signal intensity was measured using standard Alpha settings on an EnSpire® Multimode Plate Reader (PerkinElmer).

Measurements are expressed as technical duplicates (mean+/- SD, n=2). The data corresponding to the 3 nM MET condition was subjected to a non-linear regression analysis using four-parameter sigmoidal equation using Sigmaplot software (version 13).

Cell culture

Madin-Darby Canine Kidney (MDCK, kind gift of Dr Jacqueline Jouanneau, Institut Curie, Paris, France) and Human cervical cancer HeLa cells, purchased from ATCC® (American Type Culture Collection, Rockville, MD, USA), were cultured in DMEM medium (Dulbecco's Modified Eagle's Medium, Gibco, Karlsruhe, Germany), supplemented with 10% FBS (Fetal Bovine Serum, Gibco®, Life technologies, Grand Island, NY, USA) and 1/100 of ZellShield™ (Minerva Biolabs GmbH, Germany). Twenty-four h before treatment, the medium was exchanged with DMEM containing 0.1% FBS, and cells were then treated for subsequent experiments. SKOV-3 cells were cultured in RPMI 1640 medium supplemented with 10% FBS and Penicillin-Streptomycin all purchased from Gibco/ThermoFisher Scientific.

Western Blots

The assay was performed according to Simonneau et al., 2015[34]. Hela cells were collected by scraping and lysed on ice with a lysis buffer (20 mM HEPES pH 7.4, 142 mM KCl, 5 mM $MgCl_2$, 1 mM EDTA, 5% glycerol, 1% NP40 and 0.1% SDS) supplemented with freshly added protease inhibitor (1/200 dilution, #P8340, Sigma Aldrich) and phosphatase inhibitor (1/400 dilution, #P5726, Sigma Aldrich). Lysates were clarified by centrifugation (20,000 × g, 15 min) and protein concentration was determined (BCA protein assay Kit, Pierce®, Thermo scientific, IL, USA). The same protein amount (usually 20-30 µg) of cell extracts was separated by NuPAGE gel electrophoresis (4-12% Midi 1.0 mm Bis-Tris precast gels, Life technologies) and electrotransferred to polyvinylidene difluoride (PVDF) membranes (Merck Millipore). Membrane was cut between 80 and 110 kDa marker and at 50 kDa to probe simultaneously phospho or total MET, Akt and ERK. Membranes were probed overnight at 4 °C with primary antibodies diluted to 1/2000 in 5% BSA and 0.1% sodium azide in PBS using specific total MET (#37-0100 Invitrogen), total ERK2 (#SC-154 Tebu-bio), phospho-MET (Y1234/1235, clone CD26, #3077 Cell Signaling), phospho-Akt (S473, clone CD9E, #4060 Cell Signaling), phospho-ERK (T202/Y204, clone E10, #9106 Cell Signaling). After extensive wash with PBS-0.05% Tween® 20 followed incubation with anti-mouse (#115-035-146) or anti-rabbit (#711-035-152) peroxidase-conjugated IgG secondary antibodies (Jackson ImmunoResearch) diluted to 1/30000 in PBS-casein 0.2%. Protein-antibody complexes were visualized by chemiluminescence with the SuperSignal® West Dura Extended Duration Substrate (Thermo scientific) using a LAS-4000 imaging system (GE HeathCare Life Sciences) or X-ray films (CL-XposureTM Film, Thermo scientific).

AlphaScreen™ phosphorylation assay

Measurement of ERK1/2 (T202/Y204) and Akt1/2/3 (S473) activation were performed on HeLa cells using AlphaScreen SureFire Kits (#TGRES500 and #TGRA4S500) according manufacturer protocol with minor modifications. Into a 96 well plate (#353072, Flacon, Corning), 10 000 HeLa were seeded in 200 µL of DMEM supplemented with 10% FBS and let attached and grown for 24 h. Cells were next starved in DMEM supplemented with 0.1% FBS for 2 h. Cells were treated for 8 min with MET agonist from 0.3 to 300 pM with HGF/SF, K1K1 or K1K1H6 and from 3 to 3000 pM with K1H6. Cells were quickly washed in cold PBS and AlphaScreen lysis buffer was added for 15 min under middle shaking (600 rpm on orbital rocker, MixMate, Eppendorf). 5 µL of lysate in analyzed by addition of acceptor and donor bead mixes for 2 h at 23 °C. The emitted signal intensity was measured using standard Alpha settings on an EnSpire® Multimode Plate Reader. Measured are expressed has experimental duplicates (mean+/- SD, n=2). The data were subjected to a non-linear regression analysis using four-parameter sigmoidal equation using Sigmaplot software (version 13).

SKOV-3 cell migration assays.

Agonist-induced cell migration was measured by seeding 50,000 SKOV-3 cells resuspended in serum-free RPMI supplemented with 0.1% BSA (BioFroxx) in each of the upper wells of a 96-well Boyden chamber (AC96, Neuro Probe). HGF/SF, K1K1, K1K1S2, and K1K1S4 was loaded in the lower compartment and cells were left to migrate in a humidified 37°C incubator with 5% CO2 for six hours. Afterwards, non-migrated cells were removed, the cells migrated over the collagen coated (100 µg/mL Purecol, Nutacon) 8 µm pore-size membrane (Neuro Probe) were fixed in 4% paraformaldehyde in PBS and stained using HCS CellMask™ Green stain (ThermoFisher Scientific). Fluorescent intensity was measured using an Azure C600 (Azure Biosystems) and migration was quantified after control-adjustment and charted in Prism (Graphpad).

Madin-Darby canine kidney (MDCK) scatter assay

The assay was performed according to Simonneau et al., 2015[34] and Stoker et al., 1987[6]. MDCK cells were seeded at low density (2,000 cells/well on a 12-well plate, #353043 Falcon, Corning) in DMEM supplemented with 10% SVF to form compact colonies. After treatment, when colony dispersion was observed and the cells were fixed and colored by Hemacolor® stain (Merck, Darmstadt, Germany) according to the manufacturer's instructions. Representative images were captured using a phase contrast microscope with 40× and 100× magnification (Nikon Eclipse TS100, Tokyo, Japan).

Morphogenesis Assay

Wells of a black thin clear bottom 24-well plate (#4ti-0241,Brooks Lifesciences) were coated with 200 µL of 2 mg/mL type 1 rat tail collagen (354249, Corning/BD Biosciences) diluted in DMEM equilibrated in 1/10 v/v of 7.5% sodium bicarbonate solution (#25080-060, Gibco, ThermoFisher). Cells (500-700)

were seeded into a 500 µL layer of a 1:1 collagen/Growth Factor Reduced Matrigel™ (#354230, Corning/BD Biosciences) mixed in DMEM balance with bicarbonate and were treated twice a week for one month. The cells were then fixed for 24 h with 4% paraformaldehyde in PBS, colored for 3 h with 0.1 mg/L Evans Blue in PBS (#E2129, Sigma Aldrich), extensively wash in PBS and finally nuclei stained with 3 nM DAPI is PBS. Cell were observed using inverted microscope observed and confocal microscope (LSM880 Zeiss) with long distance 10× objective using 488 nm excitation Argon laser and LP 500-750 nm emission filter. 3D reconstitutions (14 µm slices) and maximum intensity projections of z-stack were realized with Zen (v8.1) software.

Survival Assay

In a clear bottom 96-well plate (#353072, Flacon, Corning), 12,500 MDCK cells were seeded and incubated for 24 h in DMEM supplemented with 10% FBS. The culture media was next added with increasing concentrations of the HGF/SF, K1K1, K1K1H6 and NK1 agonists together with the apoptosis inducer anisomycin (1.4 µM) for 15 h. The cells were then washed with PBS to eliminate dead cells and then incubated for 1 h in 200 µL of HBSS (#14025092, Gibco, ThermoFisher) containing 100 µM of Resazurin (#B21187, Sigma Aldrich). Fluorescence was then measured with Envision multimode reader (Ex: 560 nm, Em: 590 nm) with maximal signal gain set (90%) on control cells wells and on top/top reading configuration. The data were subjected to a non-linear regression analysis using four-parameter sigmoidal equation using Sigmaplot software (version 13).

In vivo MET activation in liver

All experimental procedures were conducted with the approval of the Ethics Committee for Animal Experimentation of the Nord Pas de Calais Region (CEEA 75). For kinetic analysis, 8-week old FVB mice weighing 19-21 g (Charles River) were intraperitoneally injected with K1K1 (5 µg/mouse) and sacrificed after 10, 30, 60 or 90 min of treatment. For dose-response analysis, 8-week old FVB mice weighing 19-21 g (Charles River) were intraperitoneally injected with 0.1, 0.5, 1 and 5 µg of K1K1 diluted in 100 µL of PBS and sacrificed per cervical dislocation 10 min after injection. To analyze the effect of the route of administration, 12-week old C57BL/6 NRJ mice weighing 19-21 g (Janvier Labs) were intraperitoneally or intravenously injected with K1K1 (5 µg/mouse) and sacrificed after 10 min of treatment. Livers were immediately perfused with PBS supplemented with protease and phosphatase inhibitors, collected and then rapidly frozen in liquid nitrogen for subsequent protein extraction and Western blot analysis.

Results

Rational for the design of K1K1. The generation of a recombinant covalent dimer of two HGF/SF kringle 1 domains, designated K1K1, was based on our observation that streptavidin-induced multimerization of a single HGF/SF kringle 1 domain (biotinylated synthetic kringle 1, K1B) resulted in a complex with potent biological activities similar to HGF/SF[34] which we combined with our profound understanding of ligand-receptor binding based on structural information on complexes of the MET receptor fragment with NK1 and full-length HGF/SF, obtained in our lab (manuscripts in preparation, [35]). The design of recombinant K1K1 was aimed at reproducing the spatial positions of the two HGF/SF kringle 1 domains as observed in the crystal structure of the NK1 dimer[23,36]. Consequently, the resulting covalent kringle 1 dimer no longer dependents on dimerization for its biological activity, as is the case for wild-type NK1[37,38]. Furthermore, expression in bacterial inclusion bodies offers an inexpensive and abundant source of recombinant protein with relatively few contaminants.

HGF/SF is a large protein with a complex domain structure similar to plasminogen[39]. It has an N-terminal domain (N), four copies of the kringle domain (K) and a proteolytically inactive C-terminal domain homologous to a serine protease (SPH) (Fig. 1A). HGF/SF is produced as an inactive single-chain precursor protein that, although able to bind the MET receptor, needs proteolytic cleavage to become biologically active. The α-chain remains disulfide-linked to the β-chain which comprises the SPH domain. The main, high-affinity receptor binding site is located within the first kringle domain (K1) while a second receptor binding site is present in the serine SPH domain[33,39,40].

The crystal structure of NK1 presented a head-to-tail homodimer of two NK1 monomers in which the receptor binding sites of the two kringle domains are exposed on opposite sides of the dimer[23,36]. Within this NK1 dimer structure, the distance between the carboxyl carbon of the last cysteine in one kringle and the nitrogen of the first cysteine in the other kringle is only 9 angstroms. Moreover, within the kringle domain, one of the three characteristic disulfide bonds is formed between the first and the last cysteine, the two residues that define the start and end of the kringle domain sequence and therefore the C- and N-terminus of the domain are locked in close proximity on the opposite side of the MET-binding interface. We could therefore design a linker that was sufficiently long to bridge the distance between both NK1-dimer kringle domains and chose the naturally occurring, four-amino acid long linker, SEVE, present between kringle 1 and kringle 2 in HGF/SF. This sequence was also repeated at the C-terminus as it is present in native NK1. A poly-histidine tagged variant, designated K1K1H6, was produced to facilitate binding assays together with a single kringle domain with poly-histidine tag (K1H6) produced as a "monovalent" control. We finally generated two variants with reduced affinity for heparin (K1K1S2 and K1K1S4).

Upon expression in *Escherichia coli*, K1K1 was abundantly present in inclusion bodies. Expression at lower temperature and induction with a low IPTG concentration (0.1 mM) did not favor soluble expression but instead allowed the production and extraction of folded protein from the inclusion bodies using a mild arginine-based extraction method which is based on the work of Jevševar and

colleagues[41] and subsequent work by Singh et al.[42]. Since the intrinsic heparin binding affinity of the kringle domain is dependent on the proper fold of the domain, heparin Sepharose® affinity chromatography provided an effective single-step purification of folded protein after extraction from the inclusion bodies (Figure S1A). After size exclusion chromatography, UPLC-MS analysis confirmed the purity and the congruence between predicted and observed molecular mass for each protein as is shown in Figure S1B and S1C for K1K1 and K1K1H6 respectively. Figure S1D shows all purified recombinant proteins used in this study on Coomassie-stained gel in reducing condition.

Crystallization and overall structure. Purified proteins were used to set up crystallization experiments using commercial sparse matrix screens and several conditions resulted in the growth of protein crystals at 17°C within days. Crystals were taken for X-ray diffraction experiments using a microfocus beam at the ESRF in Grenoble, France, and resulted in the collection of complete datasets and determination of the molecular structures at 1.6 Å resolution (Figure 1B) and 1.8 Å for K1K1 and K1K1H6 respectively. Both proteins crystallized in space group P 1 2_1 1 with K1K1 having two molecules per asymmetric unit and K1K1H6 only one. In addition, in K1K1H6 both kringle domains had a HEPES molecule bound to a groove which is analogous to the lysine binding pockets found in proteins such as plasminogen (Figure 1C). This HEPES molecule originates from the crystallization condition and was also found in crystal structures of NK1 obtained in our lab and in several obtained by others[25,36,43,44]. Structurally, K1K1 with and without poly-histidine tag are very similar, having a backbone root mean square deviation (RMSD) of 0.9 or 1.8 Å (Figure 1C), depending on which of the two molecules in the asymmetric unit of K1K1 is used for alignment with K1K1H6 excluding the six additional histidines. Both proteins show an elongated “stretched-out” conformation with the MET binding sites exposed at opposite ends and the N- and C-terminus located at the center. In K1K1H6, good electron density was also observed for the poly-histidine tag as His172, His173, His175, and His177 make polar contacts with residues Ala4, Asn5, and Thr17 of the N-terminal kringle domain.

Both proteins show a 180-degree rotational symmetry around a central axis presenting both receptor binding sites, made up of residues Ile34, Glu37, Ser39, Leu41, Ser44, Arg59, Glu61, Glu62, Pro72, Glu73, Arg75, and Tyr76 in the first kringle and residues Ile117, Glu120, Ser122, Leu124, Ser127, Arg142, Glu144, Glu145, Pro155, Glu156, Arg157, and Tyr158 in the second kringle, in nearly identical orientation on either side of the molecule. These residues are equivalent to NK1 residues Ile156, Glu159, S161, Leu163, Ser166, K170, Arg181, Glu183, Glu184, Pro194, Glu195, Arg197, and Tyr198 involved in the interaction with the SEMA domain of the MET receptor. Presuming the crystal structure presents us with a biologically-relevant conformation, one can envision a binding mode in which two MET receptor monomers are brought in close proximity to each other in a nearly identical orientation towards the cell surface, suggesting the most straightforward mechanism for tyrosine kinase receptor activation possible[45]. K1K1 therefore presents the most minimalistic peptide-based receptor agonist mimicking the binding and receptor activation mechanism proposed for wild-type NK1[23] but with the important difference that ligand dimerization is not required. This covalent “mimicry” is more evident

when comparing the NK1 dimer with K1K1. Alignment of the first kringle domain of K1K1 with one of the two kringle domains within the NK1 dimer places the second K1K1 kringle close to the other NK1 kringle domain (Figure S2A). However, due to the straightened conformation, the second K1K1 kringle domain is rotated by 109.7 degrees and is moved outwards by roughly 14 Å compared to the second kringle domain in the NK1 dimer (Figure S2B).

***In vitro* data.** The potency of a complex consisting of streptavidin-linked biotinylated synthetic K1 domains was well demonstrated by our laboratories in *in vitro* and *in vivo* experiments, with MET receptor activation and biological activities similar to HGF/SF[34]. To analyze MET receptor activation and downstream signaling of K1K1, Hela cells were incubated for 10 min with recombinant human HGF/SF, K1K1, K1K1H6, and monovalent K1H6 at different concentrations. MET receptor phosphorylation and activation of the key downstream signaling molecules Akt and ERK were analysed by Western blot. Figure 2A shows the resulting blot in which HGF/SF is still the most potent in stimulating MET phosphorylation when Akt, and ERK are already fully activated. Both K1K1 and K1K1H6 stimulate phosphorylation of the pathway down to the lowest tested concentration of 100 pM with a potency similar to HGF/SF at 10 pM. As predicted, treatment with K1H6 is indistinguishable from the negative control treatment. We then performed an ALPHAScreen™ analysis to precisely quantify the activation of Akt and ERK in HeLa cells stimulated with HGF/SF, K1K1, K1K1H6, and K1H6 by measuring phosphorylation levels. For p-Akt, both K1K1H6 and K1K1 show similar phosphorylation in the low nanomolar range with no significant effect caused by the presence or absence of the poly-histidine tag. Compared to HGF/SF both variant however show lower maximum activation values of Akt (Figure 2B). Interestingly, activation of the Ras-Raf-MAPK pathway as measured by the phosphorylation of ERK showed no significant differences between the stimulation by HGF/SF, K1K1H6 or K1K1 at the tested concentrations. Again, no activity was observed with K1H6 even at very high concentrations. Using the ALPHAScreen™ technology, we also confirmed the strong binding capability of K1K1H6 to recombinant human MET-Fc chimera, a soluble dimeric protein comprising the whole extracellular part of the MET receptor (MET922 fused to human IgG1). In this configuration (His-Tag/Ni-TNA and Ig-Fc/Protein A interactions) an apparent KD of the K1K1H6/MET-Fc complex cannot not be calculated (Figure 2D and Fig S3A). Therefore, to determine KD, we performed a full kinetic analysis of K1K1 and NK1 binding to immobilized MET567 using surface plasmon resonance on a Biacore T200 and measured an apparent KD of 205 nM, equivalent of this of NK1 (Figure S3B).

Having established MET receptor binding and remarkably potent activation of the MET signaling pathway by both K1K1 and K1K1H6, we subsequently focused on demonstrating the potency of inducing various biological phenotypes. We first performed a cell viability assay based on metabolic activity (resazuring assay, [46]) on MDCK cells incubated overnight (16 hours) in the presence of apoptosis inducer (anisomycin) which prevents protein synthesis and leads to cell death[47]. We looked at the cell survival after the addition of HGF/SF, K1K1, K1K1H6 and NK1 at different concentrations during anisomycin treatment (Figure 2E). HGF/SF was most effective in preventing cell death but both

K1K1 and K1K1H6 were better than native NK1 in this assay. We also used this assay to validate the specific activities of different preparations (batches) of K1K1 and K1K1H6 showing undistinguishable batch-to-batch variation and similar activities when compared to HGF/SF and NK1 (Figure S4A). Finally, MDCK scatter assay[48] is also a very sensitive assay that determines the minimal concentration at which a MET receptor agonist can induce an epithelial to mesenchymal transition shown as a morphological change and increased motility cells that under normal conditions grow in tight colonies. K1K1 was able to still exert an effect at a concentration ten times lower than that of native HGF/SF, down to 1 pM, a concentration one thousand times lower than that of NK1 (Figure S4B).

***In vivo* activation of MET signaling.** With the *in vitro* assays clearly demonstrating the potency of K1K1, superior to NK1 and in several assays, matching or even surpassing native HGF/SF, we were keen to start several *in vivo* mouse studies to look at the effects of K1K1. We first confirmed that the injection route, intraperitoneal (IP) versus intravenous (IV), did not affect the biological availability and activity in the mouse liver by establishing phosphorylation of the MET receptor, AKT and ERK by Western blot after only 10 minutes (Figure S5). For convenience and since no significant difference between the administration routes were observed, 8-week old FVB mice were IP injected with different amounts of K1K1 (0.1 to 5 μg) after which the animal was sacrificed 10 minutes later and proteins were extracted from a liver homogenate to check the phosphorylation status of the MET signaling pathway. Control as well as 0.1 μg of K1K1 did not result in any detectable MET, AKT, and ERK phosphorylation signal while injection of 0.5, 1, and 5 μg gave uniform activation of the pathway (Figure 3A). A second experiment in which 5 μg of K1K1 was injected to determine the duration of the stimulation by sacrificing the animals at 10, 30, 60, and 90 minutes, showing a diminishing signal over time and detectable up to 60 min (Figure 3B).

Role of heparan sulfates binding sites in K1K1. Having clearly demonstrated the remarkable potency of recombinant K1K1 in cell-based assays and having confirmed the potent activation of MET in the liver, a potential target organ, we set out to understand better the underlying receptor activation mechanism and potential roles of the co-receptor heparan sulphate (HS).

We first performed small angle x-ray scattering (SAXS) experiments to establish the solution behavior of K1K1 alone, in complex with heparin, and in complex with the MET567 receptor fragment in the presence or absence of heparin. In solution, K1K1 was homogenous and well-folded as judged by the radius of gyration (Rg), the size-exclusion (SEC) profile, and the Kratky plot. Interestingly, while the SAXS envelope is compatible with the K1K1 crystal structure volume-wise, it does not support the straightened conformation but instead shows a bent conformation (Figure 4A). This is also evident from comparing the experimental scatter curve with one generated based on the crystal structure using CRYSOL (Figure S6). MET567 alone also gave excellent SAXS data collection with a mass corresponding to a monomer (69.3 kDa as measured) in solution. K1K1 in complex with MET567 presents two different peaks on SEC, the first of which contains very large species and possibly

aggregates while the second presents a homogenous species with a molecular mass of 86.8 kDa, matching a 1:1 complex. The SAXS envelope presents a globular object with a "panhandle" protruding which perfectly accommodates K1K1 bound to MET567 (Figure 4B). A model based on the alignment of K1K1 with the crystal structure of NK1 in complex with MET567 obtained by our lab, produced a scatter curve that matched the experimental scatter curve remarkably well (Chi^2=3.6) (Figure S5). As several glycosylation sites are present in MET567 which could not be included in the model building process, we believe the overall structure presents a very reliable model for the K1K1-MET567 complex. In a previous study in which we investigated the kringle domain interaction with heparin and heparan sulphates, four important positively charged residues were identified; K132, R134, K170, and R181 (31) (Figure 4C). These are equivalent to the NK1 kringle residues K132, R134, K170, and R181.

The reverse charge mutations of K132 and R134 (i.e. K132E and R134E) in wild type NK1 resulted in an agonist, 1K1, with a biological activity superior to NK1 and in some assays approaching native HGF/SF[25]. While the underlying molecular mechanism remains to be understood and might be related to the complex role the HS co-receptor plays on the cell surface, we introduced the reverse charge mutations in both kringles generating two mutant K1K1 variants: K1K1S2, comprising K10E, R12E, K93E, R95E, and K1K1S4 comprising K10E, R12E, K48E, R59E in the first monomer and K93E, R95E, K131E, and R142E in the second one. These are the residues equivalent to HGF/SF residues K132, R134, K170, and R181.

In order to determine the consequences of the heparin binding site mutation, a scattering assay was performed on MDCK cells with HGF/SF, K1K1 and the two variants, allowing a qualitative comparison. In this assay there was still observable scattering activity down to 10 pM for K1K1 while K1K1S2 lost activity as a ten times higher concentration (100 pM) and K1K1S4 only showed activity in the low nanomolar range (Figure 5A). This completely unexpected result indicated that the low-affinity heparin-binding site (as opposed to the high-affinity heparin-binding site located in the N-terminal domain of HGF/SF and NK1) present in both kringle domains, does play a role in MET receptor-mediated signaling. To confirm these results obtained with the scatter assay, we also performed a 3D morphogenesis assay using the same MDCK cells (Figure 5B and Figure S7A and B) and confirmed the results obtained with the scatter assay indicating that the reverse-charge mutations affecting the heparin-binding site reduce the biological activity of K1K1S2 and K1K1S4 (Figure S7A). This loss of biological activity was quantitatively confirmed by a migration assay on SKOV3 cells (Figure 5C).

To confirm this loss of biological activity on the level of the MET receptor, we investigated the phosphorylation status of MET, AKT, and ERK. In agreement with observed phenotypes, K1K1S2 and K1K1S4 are weaker agonists that K1K1 by one and two orders of magnitude respectively (Figure S7C).

Discussion

At the end of the 19th century, Italian pathologist G Bizzozero described remarkable differences in cell turnover among different tissues and organs and proposed a straight correlation between cell turnover and regenerative potential: maximum in bone marrow, spleen and intestine, negligible in the heart and brain. More than a century after Bizzozero, the cellular basis of regeneration remains incompletely understood. The majority of post-natal tissues contain populations of 'adult stem/progenitor cells' that are capable of renewing differentiated cells of the tissue and are confined to specific micro-domains: the cell niche[49]. In an alternative strategy, tissue regeneration involves the de-differentiation of parenchymal cells, followed by expansion and re-differentiation.

The choice between these two types of regenerative responses is not clear. For example, the limited regenerative response of the mammalian myocardium to injury is mediated by cardiac stem/progenitor cells[50] whereas the response to injury of the newt or zebrafish myocardium involves de-differentiation of mature cardiomyocytes followed by expansion and re-differentiation[51]. Significantly the ability of both stem/progenitor and differentiated cell populations to respond to tissue damage is modulated by extracellular signals. Thus, if the crucial signals involved in the mobilisation and expansion of stem/progenitor or differentiated cells are understood, the prospect of enhancing tissue regeneration in response to tissue damage is considerable because the 'physiological' concentration of such signals limits, in several tissues, the regenerative response to damage.

While death rates from a number of major diseases have steadily decreased over the last ~50 years, liver mortality has increased dramatically[52]. The hepatitis B vaccine[53,54] and the recently-developed treatments for hepatitis C[55] constitute major breakthroughs, but there are half a billion people worldwide with active hepatitis B or C[56] and it may take decades to bring the burden of viral liver disease under control. Further, nearly half the deaths due to liver cirrhosis and cancer are caused by alcohol, fat or drugs and not by viruses[3]. The next challenge in liver disease, therefore, is fibrosis/cirrhosis[57], the convergent outcome of long-term liver damage, the prevention of which is a major unmet medical need.

Thus, short of removing the primary cause of liver damage, rational therapy of liver fibrosis/cirrhosis should aim to limit hepatocyte death and promote hepatocyte regeneration, thus inhibiting inflammation and activation of stellate cells and myofibroblasts. There are no therapies on the market targeting specifically the pathogenetic mechanisms underlying liver fibrosis/cirrhosis but a number of therapeutic approaches are under development, including: (i) inhibitors of cell death pathways[58] and of RIP1-3, such as necrostatin-1[11,59], (ii) galectin inhibitors[60,61], (iii) inhibitors of TGF-β, a key inducer of extracellular matrix synthesis by stellate cells/myofibroblasts[62] and, (iv) inhibitors of collagen synthesis or cross-linking including inhibitors of prolyl 4-hydroxylase[63] or antibodies blocking Lysyl oxidase

homolog 2 (LOXL2) and, (v) liver transplantation, the only curative treatment for liver cirrhosis that was available to less than 15,000 people worldwide in 2010[64,65], a year in which more than one million people died because of the disease[3].

Lineage tracing experiments have recently revealed that liver regeneration is due primarily to proliferation of surviving hepatocytes[66]. At least in mice, this process depends on HGF/SF and MET and cannot be compensated by other signalling pathways. Further, HGF/SF-MET signalling inhibits Fas-dependent hepatocyte apoptosis/necroptosis by sequestering/ inactivating the Fas receptor[67], inhibits synthesis of TGF-β[68], the key mediator of liver fibrosis, and induces apoptosis in both stellate cells[69] and myofibroblasts[70], the sources of TGF-β in damaged liver and the cells responsible for the synthesis of extracellular matrix. In essence, the large body of available mouse genetic data, combined with experimental studies of liver damage in both wild-type and knock-out mice have demonstrated unequivocally the essential physiological roles in development and regeneration and the severe organ pathology induced by failing HGF/SF-MET signalling, namely: hepatocyte death, lack of hepatocyte regeneration, inflammation and fibrosis. These data provide a strong rationale for MET agonists in liver disease, a concept now validated both at preclinical and clinical levels (see below).

Experimental evidence for therapeutic efficacy in disease model. In acute toxic liver disease HGF/SF - the physiological MET ligand - enhances survival and reduces hepatocyte death. If administered at the time of liver surgery, HGF/SF enhances liver size and liver function[71]. In cirrhotic animals it enhances both regeneration and survival after partial hepatectomy[72,73]and can both prevent and reverse fibrosis[74–76], pointing to a therapeutic role in prevention or amelioration of chronic liver disease.

Current evidence for therapeutic effect in man: In the west HGF/SF has not been used therapeutically in man, but observations have been made in Asia. Cui and colleagues identified 21 trials enrolling nearly 6000 patients, all reported in Chinese journals, on the use of HGF/SF in liver failure[77] (Fig 3e). Whilst the need for further trials remains, it is striking that overall mortality in the Chinese patients was significantly reduced when recombinant HGF/SF was administered daily and intra-venously for one month (treatment reduced the risk ratio of death by nearly half, from 1.0 - no effect - to 0.62, 95% CI 0.59-0.66). Reductions were seen in acute liver failure, sub-acute liver failure, acute-on-chronic liver failure (mainly in sub-acute liver failure) and in patients treated at an early stage of liver failure. Reported adverse effects were mild (rash, headache and fever) and non-critical. The available data therefore strongly indicate that HGF/SF constitutes an effective approach for the treatment of liver fibrosis/cirrhosis.

Outside China, a Phase I/II study of recombinant HGF/SF in fulminant liver failure reported 5 patients treated without significant side-effects, at the start of a dose-escalation study[78].

Acknowledgments

We thank SATT Nord (France) for financing the proof of concept experiments, Thierry Chassat from the PLETHA animal Facility in Lille Pasteur Institute for helpful advises and kind availability.

We would also like to thank Dr Dimitri Y. Chirgadze at the department of Biochemistry, University of Cambridge, UK, for his help in solving the structure of K1K1 and K1K1H6 and are grateful for his support and contributions to our work over the many years we collaborated.

Figure Legends:

Figure 1. Domain architecture of MET agonists and crystal structure of K1K1 and K1K1H6.
(A) Schematic representation of HGF/SF, NK1, K1K1, K1K1 variants and MET receptor full length or MET567. Amino-acid position of functional domains are indicated above boxes. CR: cysteine rich, Ig: immunoglobulin like, SPH: serine protease homology, S-S: disulphide bonds, TK: tyrosine kinase, TM: transmembrane domain. (B) The overall structure of K1K1 showing the straightened conformation of the two kringle domain and the N-terminus (blue) and C-terminus (green) located centrally with the linker. (C) Alignment of K1K1 (green) and K1K1H6 (cyan) showing a nearly identical overall structure (RMS=1.8 Å) with the C-terminal poly-histidine tag making contacts with the N-terminal kringle domain.

Figure 2. In vitro activity of the HGF/SF, K1K1, K1K1H6, and K1H6.
(A) Phosphorylation analysis by Western blot on Hela cell lysates after stimulation with ligands for 10 min at concentrations indicated above each lane. Loading controls are based on total MET, total Akt, and total ERK present in each lane. (B) AlphaScreen™ measurement of p-Akt and (C) p-ERK activation in HeLa cells after 10 min stimulation with K1K1, K1K1H6, HGF/SF and K1H6. (D) Binding determination using the ALPHAScreen™ saturation binding assay. Seven concentrations of K1K1H6 were tested on several different concentrations of MET-Fc (AA 25-922) (Suppl. Fig S3A). Shown is the binding of K1K1H6 to 3 nM MET-Fc. (E) Ligand induced MDCK survival after overnight treatment with the apoptotic inducer anisomycin. Indicated is the percentage of viable cells compared to no-anisomycin treatment after exposure to HGF/SF, K1K1, K1K1H6, and NK1 at different concentrations.

Figure 3. Dose response and MET pathway activation kinetics after intraperitoneal injection.
(A) 8-week old FVB mice were injected with PBS (Ctrl) or different amounts of K1K1 after which MET, AKT, and ERK phosphorylation in liver homogenate was determined using Western blot. Mice were sacrificed 10 minutes after injection. Results are presented as experimental duplicate (n=2). (B) MET, AKT, and ERK phosphorylation were detected by Western blot at different time points after injection of 5 µg of K1K1. Results are presented as experimental duplicate (n=2) except for control and 10 min conditions. Both blots present total MET, Akt and ERK proteins as loading controls.

Figure 4. SAXS-guided models for K1K1 alone and in complex with MET567.
(A) The computed ab initio SAXS envelope is not compatible with the elongated K1K1 crystal structure (pink), but can accommodate a bent K1K1 conformation (cyan). To fit the SAXS envelope, the two kringle domains are rotated around the linker region by roughly 60°. (B) The ab initio SAXS envelope of the 1:1 complex of K1K1 and MET567 shows a "pan-handle" extension, which accommodates K1K1. The PSI domain is partially protruding from the bottom of the envelope. (C) Single kringle domains of K1K1 showing the location of the residues involved in MET binding, as defined by Lokker et al., 1994 [40] shown in blue while the reverse charge mutations affecting the heparin binding in K1K1 S2, (K10E, R12E) and those in K1K1S4, (K10E, R12E, K48E, R59E), are shown in orange.

Figure 5. Effects on cell motility, migration and morphology.
(A) MDCK cell scattering at different concentrations K1K1, K1K1S2 and K1K1S4 showing the lowest concentration at which each protein is still active and the subsequent dilution at which no more scattering is observed. HGF/SF is used as positive control to generate maximum scattering. For complete half-log dilution of agonist series, see Data Source Image File. (B) 3D reconstruction by z-stacking of fluorescence microscopy images taken of large MDCK cell colonies stimulated with 100 pM HGF/SF or 10 nM K1K1 and mutants for four weeks. The combined fluorescence of DAPI (red) and Evans blue staining (grey scale) shows the extensive morphological change and tubulogenesis induced by both proteins. (C) Boyden chamber migration assay using SKOV3 cells. Cells were treated for 6 hours with indicated concentrations of HGF/SF, K1K1, K1K1S2 and K1K1S4 after which the migrated cells were detected with CellMask™ Green stain. Migration is presented as fold increase over control/background. Error bars represent mean +/- SD based on quadruplicates (n=4).

References

1. Naghavi M, Abajobir AA, Abbafati C, et al. Global, regional, and national age-sex specific mortality for 264 causes of death, 1980–2016: a systematic analysis for the Global Burden of Disease Study 2016. *Lancet*. 2017;390(10100):1151-1210. doi:10.1016/s0140-6736(17)32152-9
2. WHO. *Global Status Report on Noncommunicable Diseases 2014*.; 2014.
3. Lozano R, Naghavi M, Foreman K, et al. Global and regional mortality from 235 causes of death for 20 age groups in 1990 and 2010: a systematic analysis for the Global Burden of Disease Study 2010. *Lancet*. 2012;380(9859):2095-2128. doi:10.1016/s0140-6736(12)61728-0
4. Ahmad A, Ahmad R. Understanding the mechanism of hepatic fibrosis and potential therapeutic approaches. *Saudi J Gastroenterol*. 2012;18(3):155-167. doi:10.4103/1319-3767.96445
5. Nakamura T, Nawa K, Ichihara A, Kaise N, Nishino T. Purification and subunit structure of hepatocyte growth factor from rat platelets. *FEBS Lett*. 1987;224(2):311-316. doi:10.1016/0014-5793(87)80475-1
6. Stoker M, Gherardi E, Perryman M, Gray J. Scatter factor is a fibroblast-derived modulator of epithelial cell mobility. *Nature*. 1987;327(6119):239-242. doi:10.1038/327239a0
7. Park M, Dean M, Kaul K, Braun MJ, Gonda MA, Vande Woude G. Sequence of MET protooncogene cDNA has features characteristic of the tyrosine kinase family of growth-factor receptors. *Proc Natl Acad Sci U S A*. 1987;84(18):6379-6383. doi:10.1073/pnas.84.18.6379
8. Bottaro DP, Rubin JS, Faletto DL, et al. Identification of the hepatocyte growth factor receptor as the c-met proto-oncogene product. *Science*. 1991;251(4995):802-804. doi:10.1126/science.1846706
9. Padela S, Cabacungan J, Shek S, et al. Hepatocyte Growth Factor Is Required for Alveologenesis in the Neonatal Rat. *Am J Respir Crit Care Med*. 2005;172(7):907-914. doi:10.1164/rccm.200504-567oc
10. Zhou D, Tan RJ, Lin L, Zhou L, Liu Y. Activation of hepatocyte growth factor receptor, c-met, in renal tubules is required for renoprotection after acute kidney injury. 2013;84(3):509-520. doi:10.1038/ki.2013.102
11. Zhou Y, Dai W, Lin C, et al. Protective Effects of Necrostatin-1 against Concanavalin A-Induced Acute Hepatic Injury in Mice. *Mediators Inflamm*. 2013;2013:1-15. doi:10.1155/2013/706156
12. Dohi M, Hasegawa T, Yamamoto K, Marshall BC. Hepatocyte Growth Factor Attenuates Collagen Accumulation in a Murine Model of Pulmonary Fibrosis. 2000;162(6):2302-2307. doi:10.1164/ajrccm.162.6.9908097
13. Mizuno S, Matsumoto K, Li M-Y, Nakamura T. HGF reduces advancing lung fibrosis in mice: a potential role for MMP-dependent myofibroblast apoptosis. *FASEB J*. 2005;19(6):580-582. doi:10.1096/fj.04-1535fje
14. Liu Y. Hepatocyte growth factor in kidney fibrosis: therapeutic potential and mechanisms of action. *Am J Physiol Physiol*. 2004;287(1):F7-F16. doi:10.1152/ajprenal.00451.2003
15. Roos F, Ryan AM, Chamow SM, Bennett GL, Schwall RH. Induction of liver growth in normal mice by infusion of hepatocyte growth factor/scatter factor. *Am J Physiol*. 1995;268(2 Pt 1):G380-6. doi:10.1152/ajpgi.1995.268.2.G380
16. Ross J, Gherardi E, Mallorqui-Fernandez N, et al. Protein engineered variants of hepatocyte growth factor/scatter factor promote proliferation of primary human hepatocytes and in rodent liver. *Gastroenterology*. 2012;142(4):897-906. doi:10.1053/j.gastro.2011.12.006
17. Hartmann G, Prospero T, Brinkmann V, et al. Engineered mutants of HGF/SF with reduced binding to

heparan sulphate proteoglycans, decreased clearance and enhanced activity in vivo. *Curr Biol*. 1998;8(3):125-135. doi:10.1016/S0960-9822(98)70059-4

18. Owen KA, Qiu D, Alves J, et al. Pericellular activation of hepatocyte growth factor by the transmembrane serine proteases matriptase and hepsin, but not by the membrane-associated protease uPA. *Biochem J*. 2010;426(2):219-228. doi:10.1042/BJ20091448
19. Gherardi E, Youles M, Miguel R, et al. Functional map and domain structure of MET, the product of the c-met protooncogene and receptor for hepatocyte growth factor/scatter factor. *Proc Natl Acad Sci U S A*. 2003;100(21):12039-12044. doi:10.1073/pnas.2034936100
20. Birchmeier C, Birchmeier W, Gherardi E, Vande Woude GF. Met, metastasis, motility and more. *Nat Rev Mol Cell Biol*. 2003;4(12):915-925. doi:10.1038/nrm1261
21. Gherardi E, Birchmeier W, Birchmeier C, Vande Woude G. Targeting MET in cancer: rationale and progress. *Nat Rev Cancer*. 2012;12(2):89-103. doi:10.1038/nrc3205
22. Niemann HH, Jäger V, Butler PJG, et al. Structure of the human receptor tyrosine kinase met in complex with the Listeria invasion protein InlB. *Cell*. 2007;130(2):235-246. doi:10.1016/j.cell.2007.05.037
23. Chirgadze DY, Hepple JP, Zhou H, Byrd R a, Blundell TL, Gherardi E. Crystal structure of the NK1 fragment of HGF/SF suggests a novel mode for growth factor dimerization and receptor binding. *Nat Struct Biol*. 1999;6(1):72-79. doi:10.1038/4947
24. Gherardi E, Sandin S, Petoukhov M V, et al. Structural basis of hepatocyte growth factor/scatter factor and MET signalling. - Supporting Information. *Proc Natl Acad Sci U S A*. 2006;103(11):10-11.
25. Lietha D, Chirgadze DY, Mulloy B, Blundell TL, Gherardi E. Crystal structures of NK1-heparin complexes reveal the basis for NK1 activity and enable engineering of potent agonists of the MET receptor. *EMBO J*. 2001;20(20):5543-5555. doi:10.1093/emboj/20.20.5543
26. Tolbert WD, Daugherty J, Gao C, et al. A mechanistic basis for converting a receptor tyrosine kinase agonist to an antagonist. *Proc Natl Acad Sci U S A*. 2007;104(37):14592-14597. doi:10.1073/pnas.0704290104
27. Tolbert W, Daugherty-Holtrop J, Gherardi E, Vande Woude G, Xu H. Structural basis for agonism and antagonism of hepatocyte growth factor. *Proc Natl Acad Sci U S A*. 2010;107(30):13264-13269. doi:10.1073/pnas.1005183107
28. Youles M, Holmes O, Petoukhov M V, et al. Engineering the NK1 fragment of hepatocyte growth factor/scatter factor as a MET receptor antagonist. *J Mol Biol*. 2008;377(3):616-622. doi:10.1016/j.jmb.2008.01.034
29. Claire Simonneau, Bérénice Leclercq, Alexandra Mougel, Eric Adriaenssens, Charlotte Paquet, Laurent Raibaut, a Nathalie Ollivier, Hervé Drobecq, Julien Marcoux, Sarah Cianférani, David Tulasne, Hugo de Jonge OM and JV, Simonneau C, Leclercq B, Mougel A, Adriaenssens E. Semi-synthesis of a HGF / SF kringle one (K1) domain scaffold generates a potent in vivo MET receptor agonist . *Supplement*. 2015:1-9. doi:10.1039/C4SC03856H
30. Ishigaki A, Aoki M, Nagai M, et al. Intrathecal delivery of hepatocyte growth factor from amyotrophic lateral sclerosis onset suppresses disease progression in rat amyotrophic lateral sclerosis model. *J Neuropathol Exp Neurol*. 2007;66(11):1037-1044. doi:10.1097/nen.0b013e318159886b
31. Lee SH, Kim S, Lee N, et al. Intrathecal delivery of recombinant AAV1 encoding hepatocyte growth factor improves motor functions and protects neuromuscular system in the nerve crush and SOD1-G93A transgenic mouse models. *Acta Neuropathol Commun*. 2019;7(1):96. doi:10.1186/s40478-019-

0737-z

32. Bai L, Lennon D, Caplan A, … AD-N, 2012 undefined. Hepatocyte growth factor mediates mesenchymal stem cell–induced recovery in multiple sclerosis models. *nature.com*.
33. Gherardi E, Sandin S, Petoukhov M V, et al. Structural basis of hepatocyte growth factor/scatter factor and MET signalling. *Proc Natl Acad Sci U S A*. 2006;103(11):4046-4051. doi:10.1073/pnas.0509040103
34. Claire Simonneau, Bérénice Leclercq, Alexandra Mougel, Eric Adriaenssens, Charlotte Paquet, Laurent Raibaut, a Nathalie Ollivier, Hervé Drobecq, Julien Marcoux, Sarah Cianférani, David Tulasne, Hugo de Jonge OM and JV. Semi-synthesis of a HGF / SF kringle one (K1) domain scaffold generates a potent in vivo MET receptor agonist. *R Soc Chem*. 2015. doi:10.1039/C4SC03856H
35. Blaszczyk M, Harmer NJ, Chirgadze DY, Ascher DB, Blundell TL. Achieving high signal-to-noise in cell regulatory systems: Spatial organization of multiprotein transmembrane assemblies of FGFR and MET receptors. *Prog Biophys Mol Biol*. 2015;118(3):103-111. doi:10.1016/j.pbiomolbio.2015.04.007
36. Ultsch M, Lokker N a, Godowski PJ, de Vos AM. Crystal structure of the NK1 fragment of human hepatocyte growth factor at 2.0 å resolution. *Structure*. 1998;6:1383-1393. doi:10.1016/S0969-2126(98)00138-5
37. Schwall RH, Chang LY, Godowski PJ, et al. Heparin induces dimerization and confers proliferative activity onto the hepatocyte growth factor antagonists NK1 and NK2. *J Cell Biol*. 1996;133(3):709-718.
38. Sakata H, Stahl SJ, Taylor WG, et al. Heparin binding and oligomerization of hepatocyte growth factor/scatter factor isoforms. Heparan sulfate glycosaminoglycan requirement for Met binding and signaling. *J Biol Chem*. 1997;272(14):9457-9463. doi:10.1074/jbc.272.14.9457
39. Donate LE, Gherardi E, Srinivasan N, Sowdhamini R, Aparicio S, Blundell TL. Molecular evolution and domain structure of plasminogen-related growth factors (HGF/SF and HGF1/MSP). *Protein Sci*. 1994;3(12):2378-2394. doi:10.1002/pro.5560031222
40. Lokker NA, Presta LG, Godowski PJ. Mutational analysis and molecular modeling of the N-terminal kringle-containing domain of hepatocyte growth factor identifies amino acid side chains important for interaction with the c-Met receptor. *Protein Eng*. 1994;7(7):895-903.
41. Jevševar S, Gaberc-Porekar V, Fonda I, Podobnik B, Grdadolnik J, Menart V. Production of nonclassical inclusion bodies from which correctly folded protein can be extracted. *Biotechnol Prog*. 2005;21(2):632-639. doi:10.1021/bp0497839
42. Singh A, Upadhyay V, Upadhyay AK, Singh SM, Panda AK. Protein recovery from inclusion bodies of Escherichia coli using mild solubilization process. *Microb Cell Fact*. 2015;14(1). doi:10.1186/s12934-015-0222-8
43. Watanabe K, Chirgadze DY, Lietha D, de Jonge H, Blundell TL, Gherardi E. A new crystal form of the NK1 splice variant of HGF/SF demonstrates extensive hinge movement and suggests that the NK1 dimer originates by domain swapping. *J Mol Biol*. 2002;319(02):283-288. doi:10.1016/S0022-2836(02)00199-7
44. Sigurdardottir AG, Winter A, Sobkowicz A, et al. Exploring the chemical space of the lysine-binding pocket of the first kringle domain of hepatocyte growth factor/scatter factor (HGF/SF) yields a new class of inhibitors of HGF/SF-MET binding. *Chem Sci*. 2015;6(11):6147-6157. doi:10.1039/C5SC02155C
45. Lemmon MA, Schlessinger J. Cell signaling by receptor tyrosine kinases. *Cell*. 2010;141(7):1117-1134. doi:10.1016/j.cell.2010.06.011
46. O'Brien J, Wilson I, Orton T, Pognan F. Investigation of the Alamar Blue (resazurin) fluorescent dye for the assessment of mammalian cell cytotoxicity. *Eur J Biochem*. 2000;267(17):5421-5426.

doi:10.1046/j.1432-1327.2000.01606.x

47. Mosmann T. Rapid colorimetric assay for cellular growth and survival: application to proliferation and cytotoxicity assays. *J Immunol Methods*. 1983;65(1-2):55-63. doi:10.1016/0022-1759(83)90303-4
48. Stoker M, Perryman M. An epithelial scatter factor released by embryo fibroblasts. *J Cell Sci*. 1985;77:209-223.
49. Mazzarello P, Calligaro AL, Calligaro A. Giulio Bizzozero: A pioneer of cell biology. *Nat Rev Mol Cell Biol*. 2001;2(10):776-781. doi:10.1038/35096085
50. Hsieh PCH, Segers VFM, Davis ME, et al. Evidence from a genetic fate-mapping study that stem cells refresh adult mammalian cardiomyocytes after injury. *Nat Med*. 2007;13(8):970-974. doi:10.1038/nm1618
51. Jopling C, Sleep E, Raya M, Martí M, Raya A, Belmonte JCI. Zebrafish heart regeneration occurs by cardiomyocyte dedifferentiation and proliferation. *Nature*. 2010;464(7288):606-609. doi:10.1038/nature08899
52. Williams R, Aspinall R, Bellis M, et al. Addressing liver disease in the UK: A blueprint for attaining excellence in health care and reducing premature mortality from lifestyle issues of excess consumption of alcohol, obesity, and viral hepatitis. *Lancet*. 2014;384(9958):1953-1997. doi:10.1016/S0140-6736(14)61838-9
53. Aden DP, Fogel A, Plotkin S, Damjanov I, Knowles BB. Controlled synthesis of HBsAg in a differentiated human liver carcinoma-derived cell line [15]. *Nature*. 1979;282(5739):615-616. doi:10.1038/282615a0
54. Skelly J, Copeland JA, Howard CR, Zuckerman AJ. Hepatitis B surface antigen produced by a human hepatoma cell line [16]. *Nature*. 1979;282(5739):617-618. doi:10.1038/282617a0
55. Ilyas JA, Vierling JM. An Overview of Emerging Therapies for the Treatment of Chronic Hepatitis C. *Clin Liver Dis*. 2011;15(3):515-536. doi:10.1016/j.cld.2011.05.002
56. WHO | Global policy report on the prevention and control of viral hepatitis. *WHO*. 2015.
57. Friedman SL, Sheppard D, Duffield JS, Violette S. Therapy for fibrotic diseases: Nearing the starting line. *Sci Transl Med*. 2013;5(167). doi:10.1126/scitranslmed.3004700
58. Witek RP, Stone WC, Karaca FG, et al. Pan-caspase inhibitor VX-166 reduces fibrosis in an animal model of nonalcoholic steatohepatitis. *Hepatology*. 2009;50(5):1421-1430. doi:10.1002/hep.23167
59. Takemoto K, Hatano E, Iwaisako K, et al. Necrostatin-1 protects against reactive oxygen species (ROS)-induced hepatotoxicity in acetaminophen-induced acute liver failure. *FEBS Open Bio*. 2014;4:777-787. doi:10.1016/j.fob.2014.08.007
60. Traber PG, Chou H, Zomer E, et al. Regression of Fibrosis and Reversal of Cirrhosis in Rats by Galectin Inhibitors in Thioacetamide-Induced Liver Disease. *PLoS One*. 2013;8(10). doi:10.1371/journal.pone.0075361
61. Traber PG, Zomer E. Therapy of experimental NASH and fibrosis with galectin inhibitors. *PLoS One*. 2013;8(12). doi:10.1371/journal.pone.0083481
62. Ling H, Roux E, Hempel D, et al. Transforming Growth Factor β Neutralization Ameliorates Pre-Existing Hepatic Fibrosis and Reduces Cholangiocarcinoma in Thioacetamide-Treated Rats. *PLoS One*. 2013;8(1). doi:10.1371/journal.pone.0054499
63. Bickel M, Barinchaus KH, Gerl M, et al. Selective inhibition of hepatic collagen accumulation in experimental liver fibrosis in rats by a new prolyl 4-hydroxylase inhibitor. *Hepatology*. 1998;28(2):404-411. doi:10.1002/hep.510280217

64. European Liver Transplant Registry - ELTR. http://www.eltr.org/. Accessed July 20, 2020.

65. UNOS (2014) United Network for Organ Sharing (http://www.unos.org/).

66. Miyaoka Y, Ebato K, Kato H, Arakawa S, Shimizu S, Miyajima A. Hypertrophy and unconventional cell division of hepatocytes underlie liver regeneration. *Curr Biol*. 2012;22(13):1166-1175. doi:10.1016/j.cub.2012.05.016

67. Wang X, DeFrances MC, Dai Y, et al. A mechanism of cell survival: Sequestration of Fas by the HGF receptor Met. *Mol Cell*. 2002;9(2):411-421. doi:10.1016/S1097-2765(02)00439-2

68. Narmada BC, Chia SM, Tucker-Kellogg L, Yu H. HGF regulates the activation of TGF-β1 in rat hepatocytes and hepatic stellate cells. *J Cell Physiol*. 2013;228(2):393-401. doi:10.1002/jcp.24143

69. YC M, HX J, JH Z, et al. [Activation of hepatocyte growth factor-induced apoptosis in hepatic stellate cells]. *Zhonghua Gan Zang Bing Za Zhi*. 2012;20(9). doi:10.3760/CMA.J.ISSN.1007-3418.2012.09.012

70. Kim WH, Matsumoto K, Bessho K, Nakamura T. Growth inhibition and apoptosis in liver myofibroblasts promoted by hepatocyte growth factor leads to resolution from liver cirrhosis. *Am J Pathol*. 2005;166(4):1017-1028. doi:10.1016/S0002-9440(10)62323-1

71. Ishii T, Sato M, Sudo K, et al. Hepatocyte growth factor stimulates liver regeneration and elevates blood protein level in normal and partially hepatectomized rats. *J Biochem*. 1995;117(5):1105-1112. doi:10.1093/oxfordjournals.jbchem.a124814

72. Nishino M, Iimuro Y, Ueki T, Hirano T, Fujimoto J. Hepatocyte growth factor improves survival after partial hepatectomy in cirrhotic rats suppressing apoptosis of hepatocytes. *Surgery*. 2008;144(3):374-384. doi:10.1016/j.surg.2008.04.011

73. Xue F, Takahara T, Yata Y, et al. Hepatocyte growth factor gene therapy accelerates regeneration in cirrhotic mouse livers after hepatectomy. *Gut*. 2003;52(5):694-700. doi:10.1136/gut.52.5.694

74. Matsuda Y. Preventive and therapeutic effects in rats of hepatocyte growth factor infusion on liver fibrosis/cirrhosis. *Hepatology*. 1997;26(1):81-89. doi:10.1053/jhep.1997.v26.pm0009214455

75. Matsuno Y, Iwata H, Umeda Y, et al. Hepatocyte growth factor gene transfer into the liver via the portal vein using electroporation attenuates rat liver cirrhosis. *Gene Ther*. 2003;10(18):1559-1566. doi:10.1038/sj.gt.3302052

76. Ueki T, Kaneda Y, Tsutsui H, et al. Hepatocyte growth factor gene therapy of liver cirrhosis in rats. *Nat Med*. 1999;5(2):226-230. doi:10.1038/5593

77. Cui YL, Meng M Bin, Tang H, et al. Recombinant human hepatocyte growth factor for liver failure. *Contemp Clin Trials*. 2008;29(5):696-704. doi:10.1016/j.cct.2008.04.006

78. Ido A, Moriuchi A, Marusawa H, et al. Translational research on HGF: A phase I/II study of recombinant human HGF for the treatment of fulminant hepatic failure. In: *Hepatology Research*. Vol 38. Hepatol Res; 2008. doi:10.1111/j.1872-034X.2008.00432.x

Figure 1

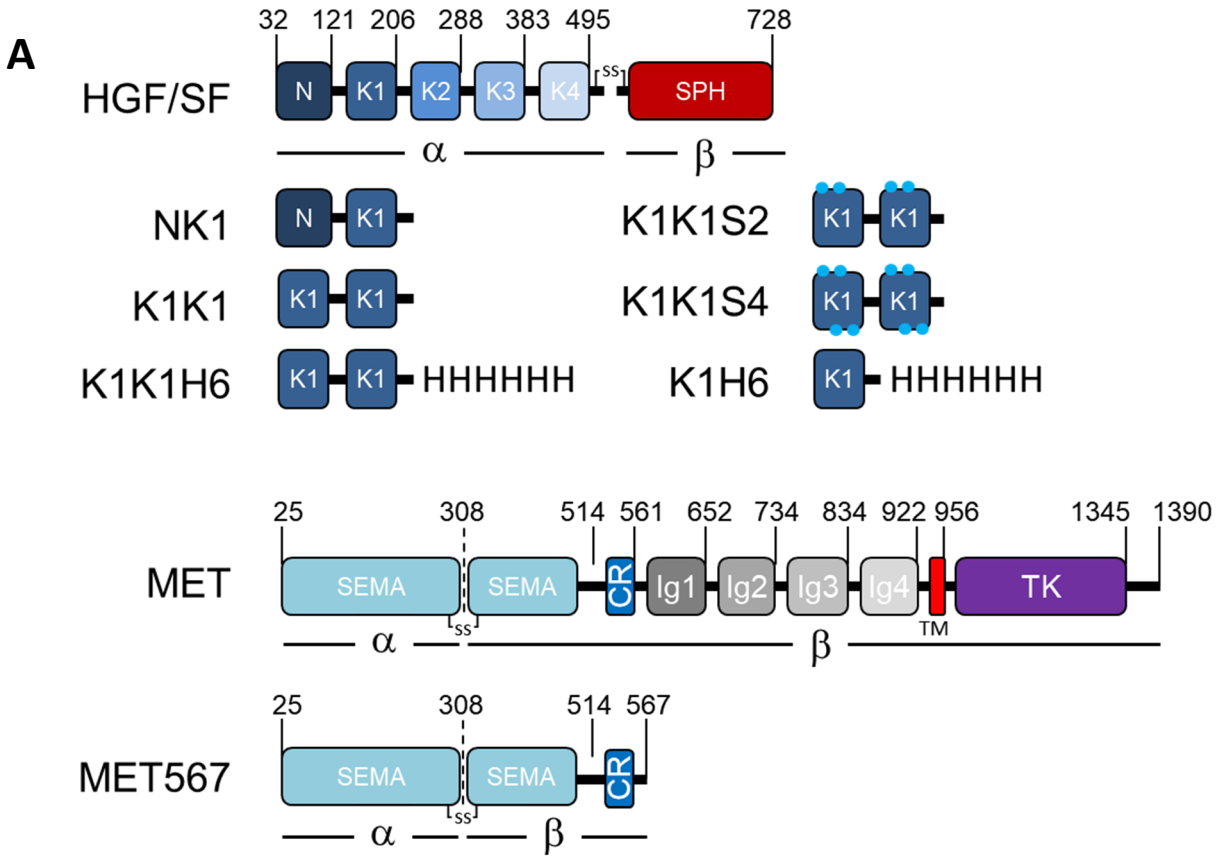

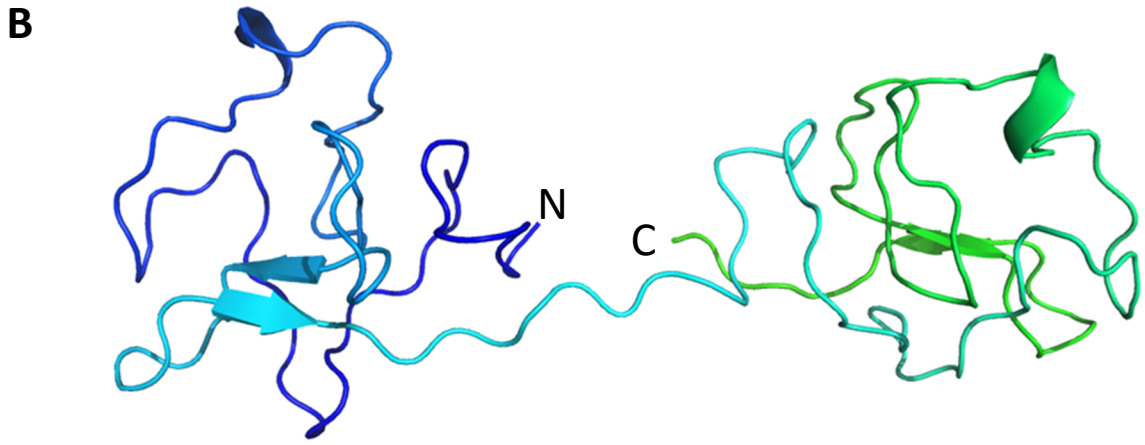

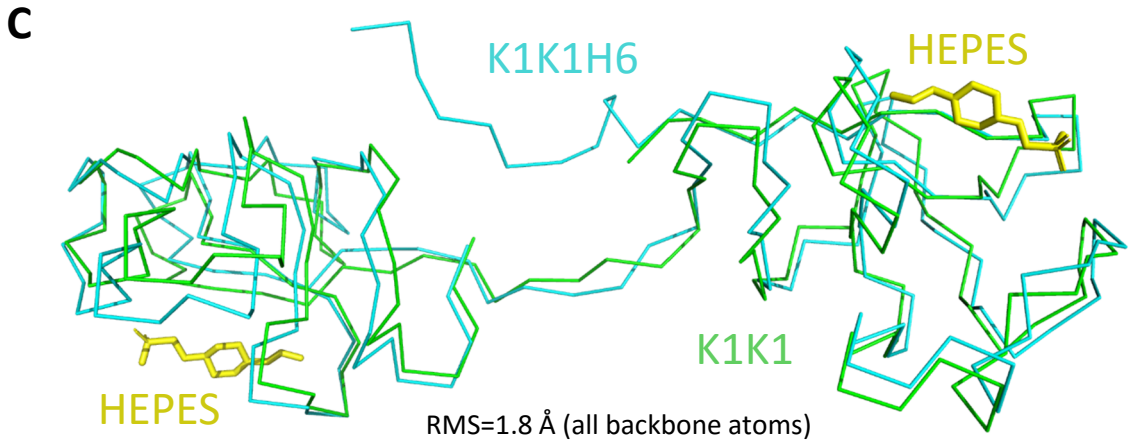

Figure 2

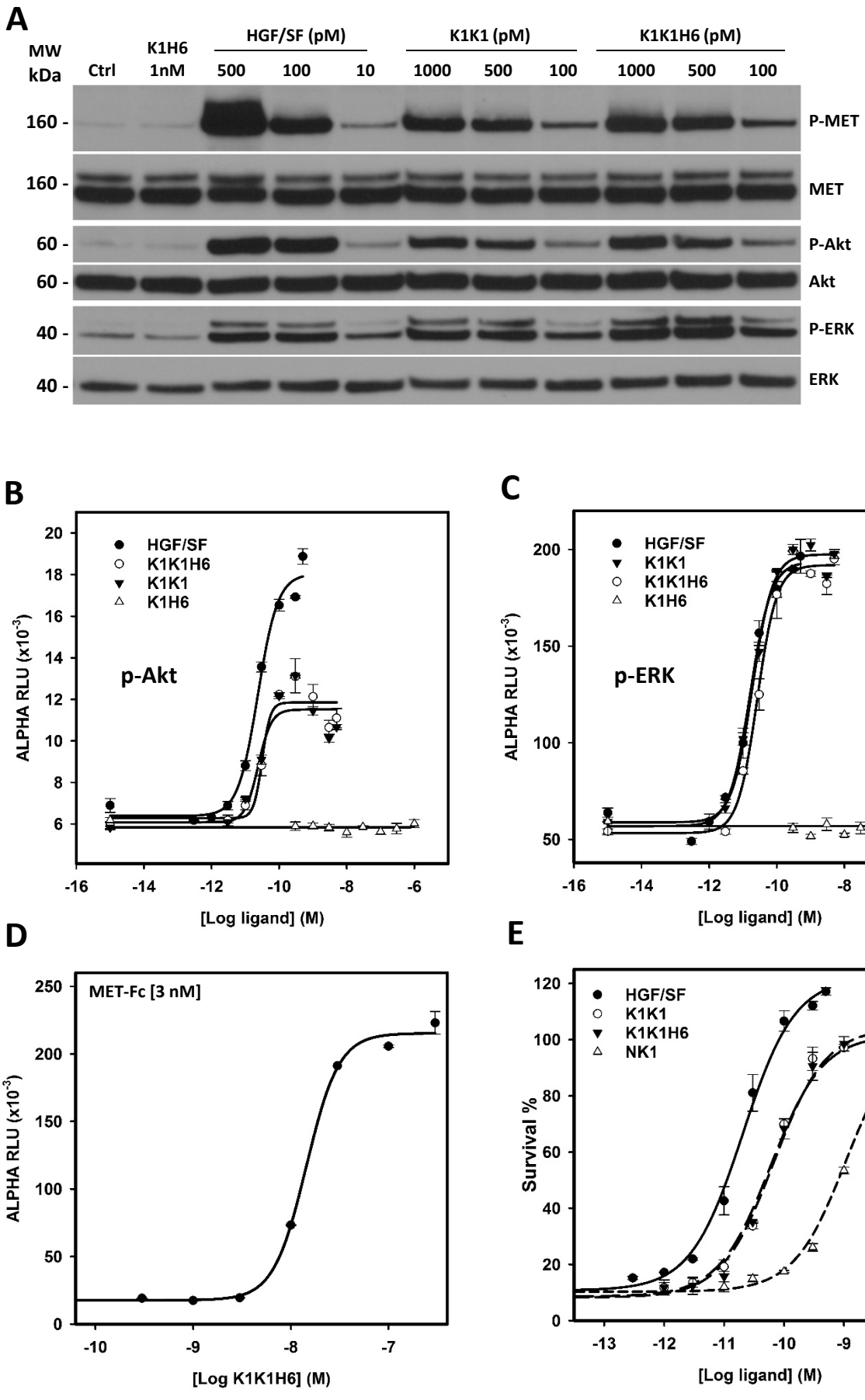

Figure 3

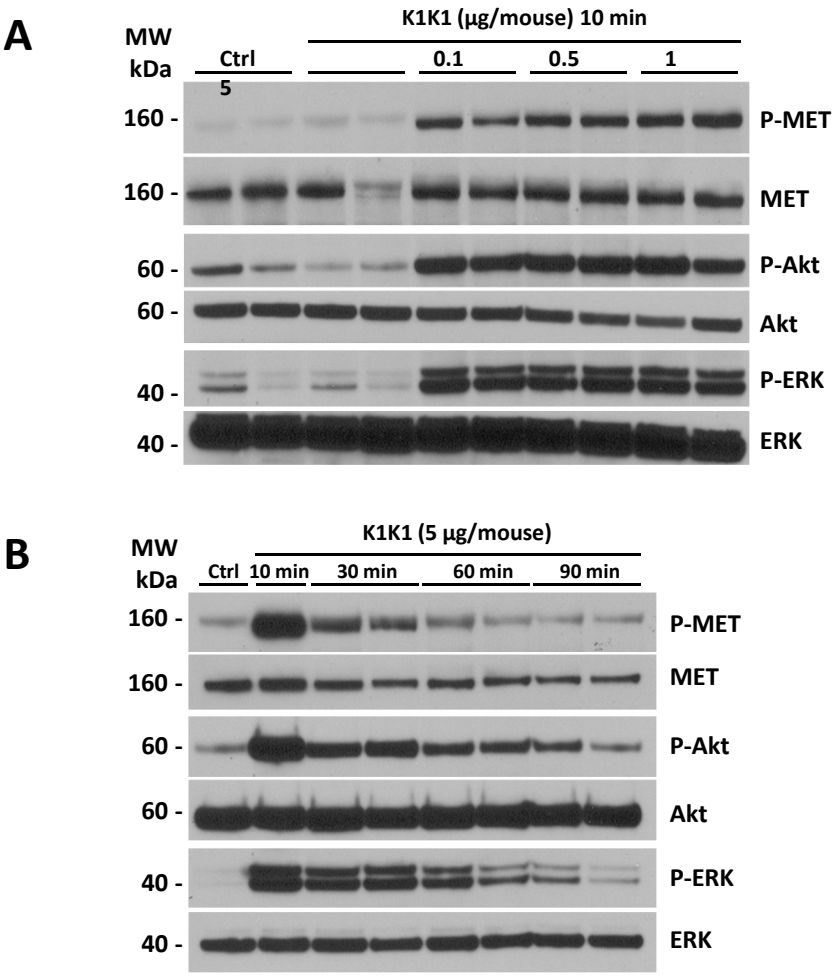

Figure 4

A

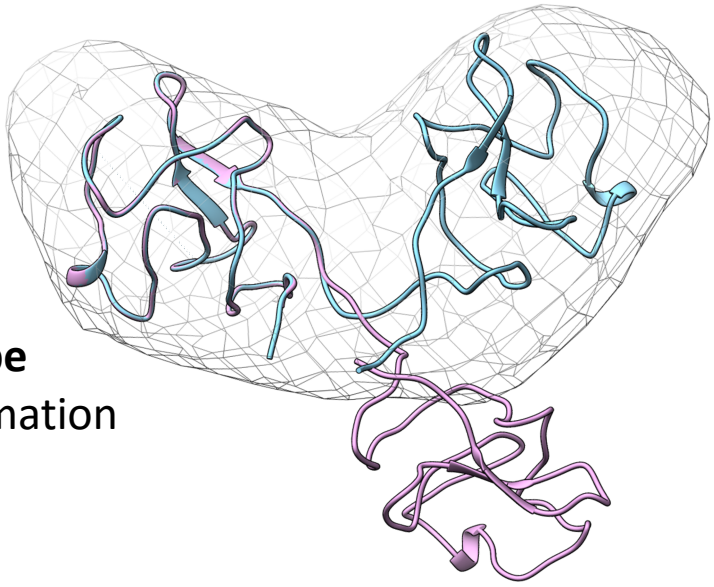

SAXS envelope
bent K1K1 conformation

B

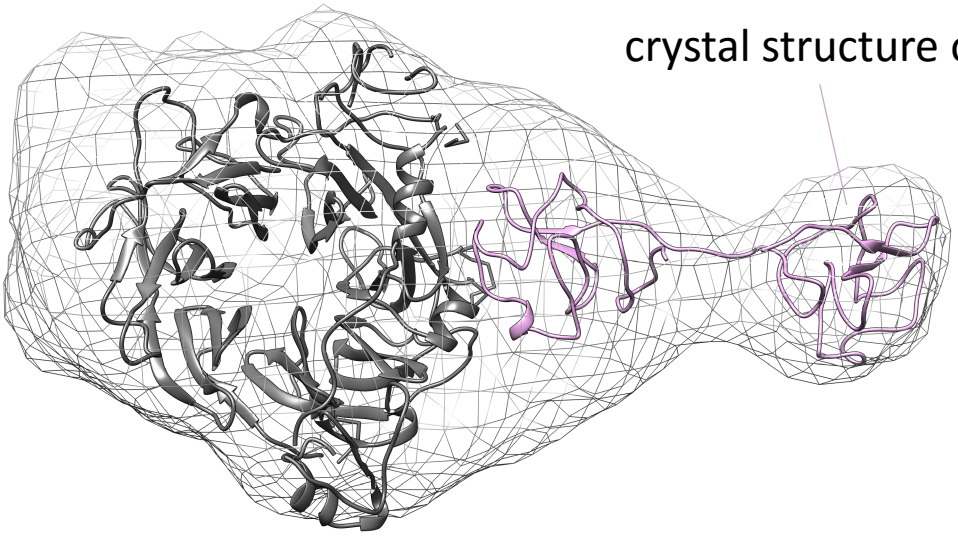

crystal structure of K1K1

C

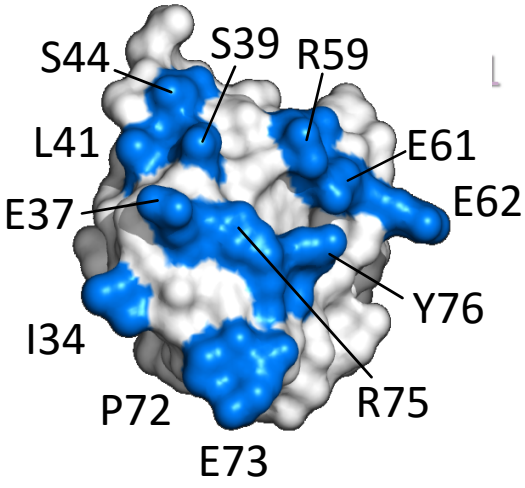

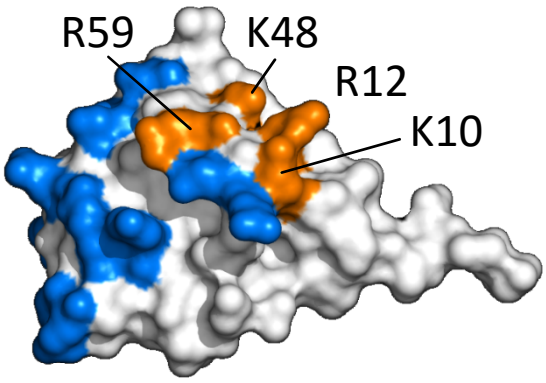

Figure 5

A

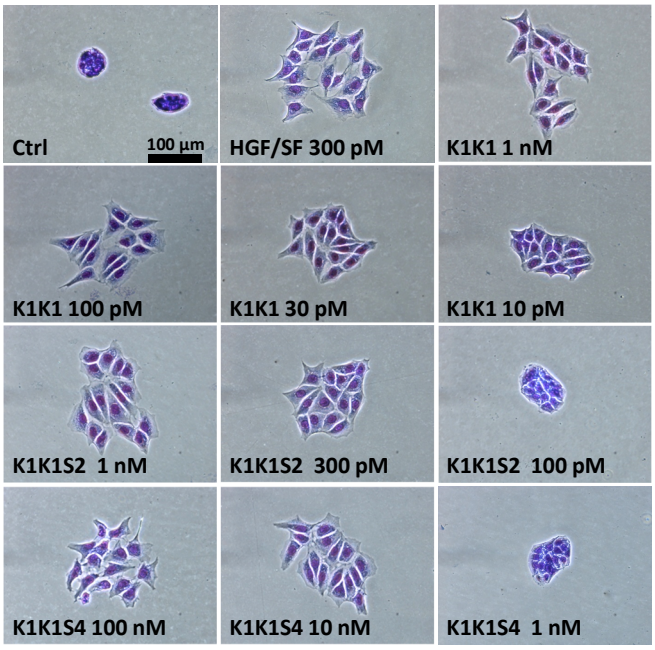

B

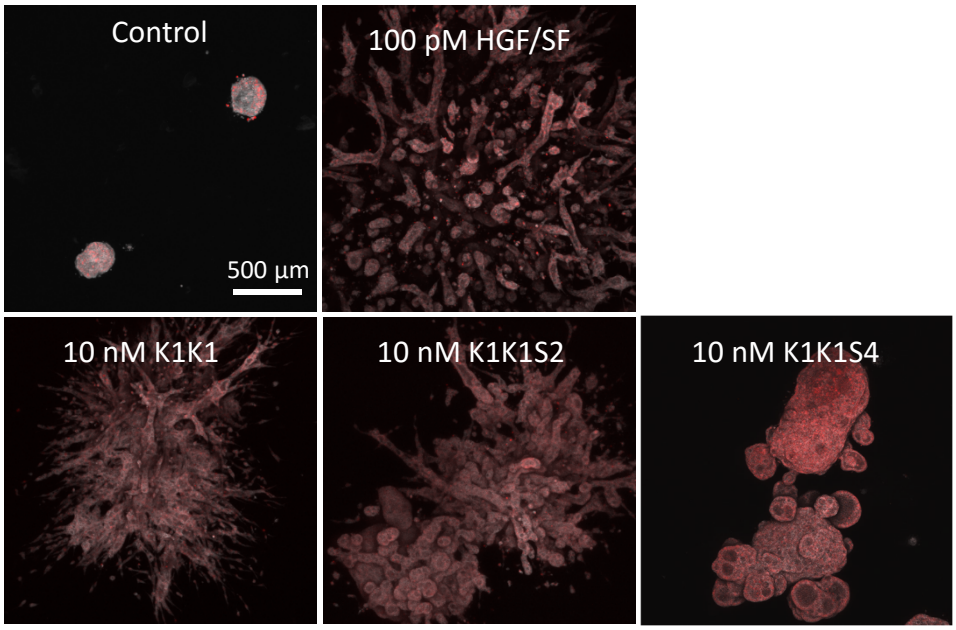

C